13th World Conference on Earthquake Engineering
Vancouver, B.C., Canada
August 1-6, 2004
Paper No. 3099

EVALUATION OF GROUND STRAIN FROM IN SITU DYNAMIC RESPONSE

Ellen M. RATHJE[1], Wen-Jong CHANG[2], Kenneth H. STOKOE, II[3], and Brady R. COX[4]

SUMMARY

Evaluating the in situ strains induced in the soil during dynamic experiments is a critical aspect of various seismic field studies. This paper compares and contrasts four approaches for evaluating in situ soil strains from field measurements of dynamic response. These approaches are either based strictly on a displacement field (displacement-based methods) or on an assumed propagating wave type (wave propagation-based methods). The displacement-based (DB) method utilizes displacement-time histories at embedded instrumentation points, along with an assumed displacement field between points, to compute shear strain. Wave propagation-methods traditionally utilize the ratio of particle velocity to wave propagation velocity to compute shear strain. An in situ field experiment, which utilized a vertically vibrating vibroseis truck to dynamically load an instrumented test area within a liquefiable soil deposit, was used to evaluate the various strain computation methods. Three wave-propagation methods were considered for this experiment: (1) plane shear wave (PSW) propagation, (2) plane Rayleigh wave (PRW) propagation, and (3) apparent wave (AW) propagation. These methods were compared with the DB method at various loading levels. The comparison shows that the PSW and PRW methods overpredict mean shear strain levels, as compared with the DB method, by 40% to 80%. These wave-propagation methods do not perform well for this experiment because they do not represent the wave type that is predominantly shearing the soil. The shear strains from the AW and DB methods compare favorably over a large range of shear strain levels (0.0005% to 0.02%). However, the AW method cannot adequately track the change in shear strain amplitude after significant pore pressure generation unless a cycle-by-cycle computation is performed. This cycle-by-cycle computation was facilitated in this study by a sinusoidal load, which may not always be the case for in situ measurements. Additionally, one must consider the dominant wave type that is shearing the soil when using any wave propagation-based method. This issue is critical for experiments that generate stress wave fields that are different than those in this study.

[1] Assistant Professor, University of Texas, Austin, TX, USA. Email: e.rathje@mail.utexas.edu
[2] Assistant Professor, National Chi-Nan University, Puli, Taiwan, Email: wjchang@ncnu.edu.tw
[3] Milton T. and Jennie C. Graves Professor, University of Texas, Austin, TX, USA. Email: k.stokoe@mail.utexas.edu
[4] Graduate Research Assistant, University of Texas, Austin, TX, USA. Email: brcox@mail.utexas.edu

INTRODUCTION

Evaluating the in situ strains induced in the soil during dynamic field experiments is critical in many seismic field studies, such as blast-induced liquefaction [Rollins et al. 1], in situ nonlinear soil property evaluation [Stokoe et al. 2, Zeghal et al. 3], and vibroseis-induced liquefaction [Rathje et al. 4]. For these field studies, the in situ dynamic response (i.e., acceleration, particle velocity) is recorded with embedded instrumentation at various points in the subsurface and used to compute strain. For geotechnical considerations, shear strain is the strain component that often is most critical, although some blast studies have considered compressive strain [e.g., Veyera et al. 5; Rollins et al. 1]. There are two general approaches to computing strain from in situ dynamic measurements: the displacement-based approach and the wave propagation-based approach. The displacement-based approach utilizes displacement-time histories at adjacent measurement points, along with an assumed displacement field between points, to compute strain. Depending on the number of measurement points and the directional components of vibration measured, it is possible to compute both compressive and shear components of strain. The wave propagation-based approach utilizes the ratio of particle velocity to wave propagation velocity to compute strain. Depending on the directional component of vibration that is recorded, as well as the wave propagation type, both compressive and shear components of strain can be computed.

Most previous geotechnical investigations that computed strain components from dynamic measurements have used displacement-based approaches. Zeghal et al. [3] estimated shear strains from downhole measurements of horizontal acceleration at the Lotung large-scale seismic test (LSST) site in Taiwan. This study used an analytical procedure that computes shear strain at a point using displacement values from three adjacent depths and an expression derived from the differential of a second-order Lagrange interpolating polynomial [e.g., Chapra and Canale 6]. This analytical procedure assumes one-dimensional wave propagation and results in strain estimates that are second-order accurate. To compute the in situ shear strains in the Zeghal et al. [3] study, the recorded acceleration-time histories were numerically integrated twice with respect to time to obtain displacement-time histories that were used in the strain computations. The downhole accelerometer array used in this investigation consisted of 4 accelerometers in the top 17 m with the vertical spacing between accelerometers equal to about 5 m. Shear strains were computed for low to moderate earthquake shaking (peak ground acceleration at the surface of 0.01 to 0.26 g) and the strains ranged from about 0.001% to 0.1%. Gohl et al. [7] computed both compressive and shear components of strain from downhole measurements of acceleration during a blast experiment. Three components of acceleration were measured at two locations separated by a horizontal distance of about 2.5 m. Double integration of the acceleration-time histories produced three orthogonal components of displacement-time histories at each measurement point. These displacement-time histories were used with small-strain mechanics theory and the relative locations of the measurement points to compute the strain components. Computed values of shear strain ranged from 0.01% to over 1.0%. These strain estimates were first-order accurate and represent average values between measurement points.

This paper compares four approaches for evaluating in situ soil strains, one displacement-based (DB) method and three wave propagation-based (WB) methods. The DB method utilizes displacements from the corners of the 4-node square array to compute strain at the center of the array. The three wave types considered for the WB methods are: (1) plane shear wave (PSW) propagation, (2) plane Rayleigh wave (PRW) propagation, and (3) apparent wave (AW) propagation. These methods are named based on the assumed wave type that is propagating through the soil: shear, Rayleigh, or apparent waves. The AW method is so named because the motion is not assumed to be one specific wave type. Each of these methods utilizes the ratio of particle velocity to wave propagation velocity to compute strain. Data from an in situ liquefaction experiment [Rathje et al. 4] were used to compare the four strain computation methods. This experiment utilizes a vertically vibrating vibroseis to dynamically load a 1.2 m by 1.2 m by

1.2 m reconstituted, liquefiable test specimen located 3.3 m (horizontally) from the vibroseis. Geophones were embedded at 5 locations within the test specimen during construction to monitor horizontal and vertical particle velocities for use in the strain computation methods.

STRAIN COMPUTATION METHODS

Displacement-Based Methods

Displacement-based (DB) strain computation methods are established strictly on solid mechanics definitions of strain, such as:

$$\varepsilon_i = \frac{\partial u_i}{\partial x_i} \tag{1}$$

$$\gamma_{ij} = \frac{\partial u_i}{\partial x_j} + \frac{\partial u_j}{\partial x_i} \tag{2}$$

where ε represents normal strain, γ represents engineering shear strain, u represents displacement, x represents direction, and i and j are direction subscripts that take on 1, 2 or 3 to represent the three, orthogonal coordinate dimensions. To compute strain, displacements are measured at known, discrete points in the soil and numerical methods are used to estimate the derivatives in equations (1) and (2). For three-dimensional problems, there are six components to strain (three normal and three shear components). For plane strain problems, only three components of strain (two normal and one shear) are relevant, while four strain components (three normal and one shear) are important for axisymmetric problems. When considering one-dimensional shear wave propagation, which is common in geotechnical earthquake engineering, only shear strain is of interest.

The experiment conducted in this study involved the vertical vibration of a circular area at the ground surface, a configuration that is axially symmetric (Figure 1a). An instrumented test area was placed along one radial ray path from the source. Within this instrumented test area, the locations of the in situ measurement points were chosen to create a 4-node rectangular array (Figure 1b). For this array, the horizontal direction is defined as x, the vertical direction is z, and the displacements measured in these

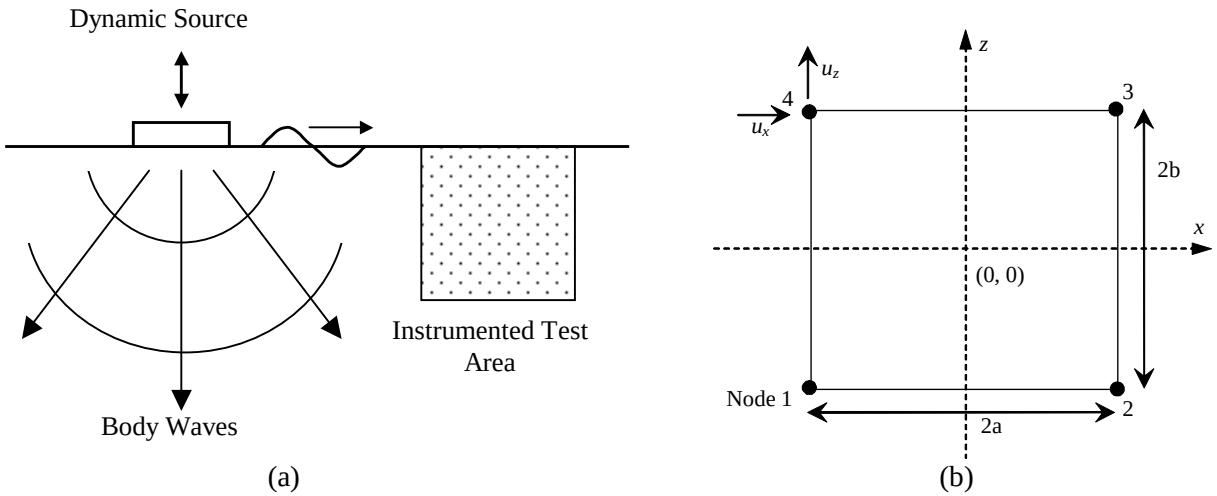

Figure 1. (a) Experimental test set up and (b) instrumentation array for strain computations.

two orthogonal directions are u_x and u_z, respectively (Figure 1b). The sides of this rectangular array measure 2a in the x direction and 2b in the z direction. Using this coordinate system, the pertinent strain components are ε_x, ε_z, and γ_{xz}.

To compute the strain components within the rectangular array, a formulation was developed that is based on the 4-node isoparametric element formulation often used in finite element analysis [e.g., Cook et al. 9]. For this formulation, the horizontal and vertical displacements (u_x and u_z, respectively) are known at the nodal points and a linear variation of displacement is assumed between nodes. The resulting expressions that describe the displacement variation across an element (element size: 2a by 2b) in terms of the nodal displacements are:

$$u_x(x,z) = \frac{1}{4}\left[u_{x1}(1-x/a)(1-z/b) + u_{x2}(1+x/a)(1-z/b) + \right.$$
$$\left. + u_{x3}(1+x/a)(1+z/b) + u_{x4}(1-x/a)(1+z/b)\right] \quad (3)$$

$$u_z(x,z) = \frac{1}{4}\left[u_{z1}(1-x/a)(1-z/b) + u_{z2}(1+x/a)(1-z/b) + \right.$$
$$\left. + u_{z3}(1+x/a)(1+z/b) + u_{z4}(1-x/a)(1+z/b)\right] \quad (4)$$

where u_{ij} is the displacement in the i direction ($i = x$ or z) at node j (j = 1 to 4), $2a$ is the size of the element in the x-direction, and $2b$ is the size of the element in the z-direction (Figure 1b). Differentiating these expressions with respect to x and z, and incorporating them into equations (1) and (2), results in the following expressions for strain at a point (x, z) within the element:

$$\varepsilon_x(x,z) = \frac{1}{4a}\left[-u_{x1}(1-z/b) + u_{x2}(1-z/b) + u_{x3}(1+z/b) - u_{x4}(1+z/b)\right] \quad (5)$$

$$\varepsilon_z(x,z) = \frac{1}{4b}\left[-u_{z1}(1-x/a) - u_{z2}(1+x/a) + u_{z3}(1+x/a) + u_{z4}(1-x/a)\right] \quad (6)$$

$$\gamma_{xz}(x,z) = \frac{1}{4}\left[-\frac{u_{x1}}{b}(1-x/a) - \frac{u_{z1}}{a}(1-z/b) - \frac{u_{x2}}{b}(1+x/a) + \frac{u_{z2}}{a}(1-z/b) + \right.$$
$$\left. + \frac{u_{x3}}{b}(1+x/a) + \frac{u_{z3}}{a}(1+z/b) + \frac{u_{x4}}{b}(1-x/a) - \frac{u_{z4}}{a}(1+z/b)\right] \quad (7)$$

These expressions provide strain values within the rectangular element at location (x, z) and are first-order accurate. It is important to note that these expressions are only applicable to rectangular elements. An arbitrary quadrilateral that has variable side dimensions requires a more complicated transformation. A detailed derivation for these strain equations, along with a more general derivation that does not require that the instrumentation array be rectangular, can be found in Chang [8].

The most critical assumption employed in this strain formulation is the linear variation of displacement between nodes. For this assumption to be valid, the wavelength of the waves traveling through the instrumentation array should be much larger than the element size. To ensure that the computed strains are not significantly affected by the linear variation assumption, it is recommended that the larger dimension of the instrumentation array be smaller than 1/5 of the wavelength.

Wave Propagation-Based Methods

Wave propagation-based (WB) strain computation methods utilize particle velocity and wave propagation velocity to compute various components of strain [e.g., Richart et al. 10]. These methods assume a one-dimensional stress wave traveling through the system. The general expression for strain based on wave propagation is:

$$Strain = \frac{-\dot{u}}{V} \tag{8}$$

where *Strain* can be either normal (ε) or shear (γ) strain, $\dot{u}$ is particle velocity, and V is wave propagation velocity. The minus sign in equation (8) indicates that the strain is 180 degrees out of phase with the particle velocity. For normal strains induced by compression waves, compression wave velocity (V_c) is used in equation (8) along with the particle velocity measured in the same direction as the direction of compression wave propagation. For shear strains induced by shear waves, shear wave velocity (Vs) is used in equation (8) along with the particle velocity measured in the direction perpendicular to the direction of shear wave propagation. These strain computations require a known direction of wave propagation and an assumed wave type.

For the experiment conducted, shear strains were of most interest and computations focused on computing this strain component. Considering the experimental set up and the location of the instrumented test area (Figure 1a), the waves generated by the dynamic source travel horizontally through the test area. Therefore, the horizontal wave propagation velocity should be used in equation (8) along with particle velocities measured in the direction perpendicular to wave propagation (i.e., vertical in this case). The wave field generated by the dynamic source is complex, with shear, compression, and Rayleigh-type surface waves traveling through the test area. However, Rayleigh waves carry the majority of energy (68%) and attenuate less rapidly ($1/R^{0.5}$, R = distance from the source) than the body waves [Woods 11]**.** Therefore, Rayleigh waves should dominate the dynamic loading for the testing program considered. However, for comparison purposes, three potential wave types were considered: plane shear waves (PSW), (2) plane Rayleigh waves (PRW), and (3) plane apparent waves (AW).

The simplest assumption would involve plane shear wave propagation. Shear strain can be easily computed using the wave velocity for a horizontally propagating, vertically polarized shear wave ($V_{S,hv}$) measured prior to testing. The resulting shear strain expression for the PSW method is:

$$\gamma_{xz} = \frac{-\dot{u}_z}{V_{S,hv}} \qquad \text{PSW method} \tag{9}$$

where $\dot{u}_z$ is the vertical particle velocity. Using the wave velocity measured before testing to compute strain assumes that the soil remains relatively linear during the entire test sequence. However, this assumption is not valid for many problems of engineering interest (e.g., liquefaction, site response under high levels of shaking).

Although assuming shear wave propagation may be most simple, it ignores that fact that shear waves are not the dominant wave type shearing the soil in this experiment (Figure 1a). Because of the location of the test area in relation to the dynamic source and because body waves attenuate more quickly than surface waves, Rayleigh-type surface waves are the dominant wave type shearing the soil. However, equation (8) is not valid for Rayleigh waves because Rayleigh waves generate both vertical and horizontal motion, and the induced displacement field varies with depth (Figure 2). To develop a valid expression for the shear

strain induced by a Rayleigh wave, the far field, analytical solution for the *x* and *z* displacement fields [Rayleigh 12] were used and incorporated into the shear strain definition in equation (2). The resulting PRW expression for shear strain, which is similar in form to equation (8), is:

$$\gamma_{xz} = \frac{\dot{u}_z}{V_R} \cdot \alpha_v \qquad \text{PRW method} \qquad (10)$$

where $\dot{u}_z$ is the vertical particle velocity, V_R is the Rayleigh wave propagation velocity, and α_v is the shear strain ratio. The factor α_v is a function of Rayleigh wave velocity, Poisson's ratio (ν), loading frequency (f), and depth [Chang 8]. Figure 3 shows the variation of α_v with normalized depth, z/λ (where $\lambda = V_R / f$), for V_R equal to 150 m/s and ν equal to 0.25. The largest values of α_v occur near the ground surface, because the displacements are varying most in this area (Figure 2). At z/λ greater than 1.0, α_v takes on a relatively constant value. Sensitivity analyses on α_v indicate that Poisson's ratio does

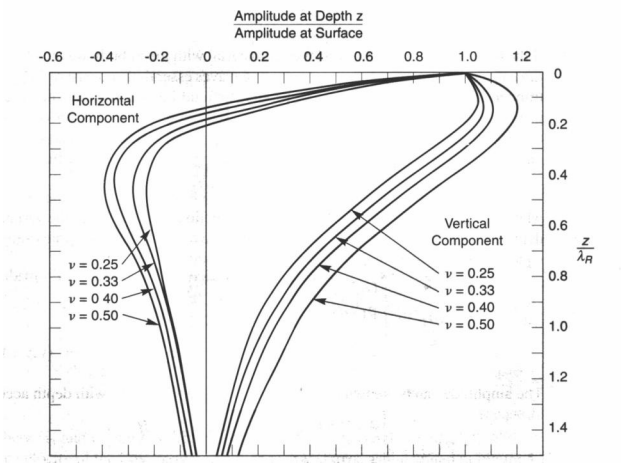

Figure 2. Variation of horizontal and vertical displacement amplitudes with depth for Rayleigh waves [Richart et al. 10].

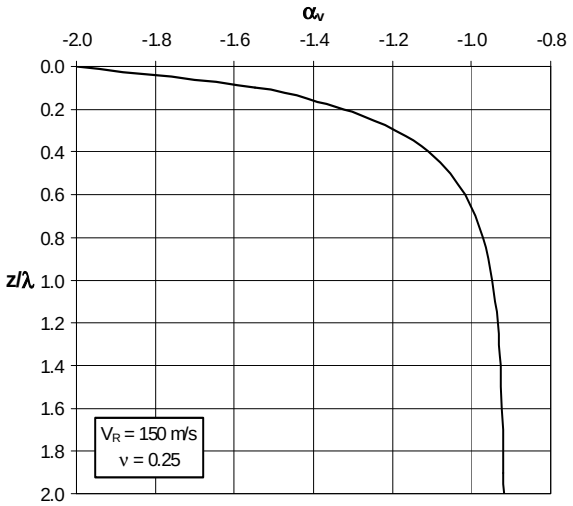

Figure 3. Variation of shear strain ratio (α_v) with depth.

not have a significant effect on the variation of α_v with depth and wave velocity has only a minor effect. Note that for the experiment performed in this study, the instrumentation was located within z/λ=0.2 of the ground surface.

Similar to the PSW shear strain computation method, the PRW method is simple and easy to use. Theoretically, only one vertically oriented geophone is required to evaluate shear strain, along with prior Rayleigh wave velocity measurements of the native soil. Conversely, two receivers can be used to monitor V_R during testing.

The last strain computation method considered is the apparent wave (AW) method. This method uses the same form of the shear strain expression as the PSW (equation 9), but uses the wave velocity measured in situ during dynamic testing. This wave velocity is called the "apparent" wave velocity because most likely it represents shearing from multiple wave types, as well as reflected waves for the test pit analyzed in this study. The resulting shear strain expression for the AW method is:

$$\gamma_{xz} = \frac{-\dot{u}_z}{V_{ah}} \qquad \text{AW method} \qquad (11)$$

where $\dot{u}_z$ is the vertical particle velocity and V_{ah} is the apparent wave velocity propagating in the horizontal direction. The in situ V_{ah} is obtained from the phase difference between two adjacent sensors separated by a horizontal distance.

SHEAR STRAIN COMPARISONS

Test Set Up

Data from an in situ liquefaction experiment [Rathje et al. 4] were used to compare and contrast the strain computation methods. This newly developed testing procedure dynamically loads an in situ soil deposit using a vertically vibrating vibroseis as the loading source. The vibroseis dynamically loads a footing at the ground surface, which generates body waves and surface waves that propagate through the soil. The experiment used in this study focused on the dynamic response of a reconstituted, liquefiable test specimen constructed in the field and located 3.3 m (horizontally) from the vibrating footing. The general set up is shown in Figure 1a, while a more detailed schematic is shown in Figure 4.

The experiment took place at an aggregate quarry in Austin, Texas. The test site is located on the flood plain of the Colorado River, where the natural soil consists of poorly-graded sand with about 5% fines. The ground water table is located 2.1 m below the ground surface and the native soil is somewhat cemented and non-liquefiable within a meter of the ground surface. The liquefiable test specimen was constructed within an excavation (1.2 m by 1.2 m by 1.2 m) that was lined with an impermeable liner. The specimen consisted of a poorly-graded aggregate sand and was constructed within the excavation by water sedimentation. The specimen preparation procedure resulted in a very loose sand specimen (relative density ~ 35%) and allowed instrumentation to be placed within the specimen during construction. The embedded instrumentation consisted of liquefaction sensors, which integrate two orthogonally-oriented geophones and a pore pressure transducer in a single acrylic case. Liquefaction sensors were embedded at 5 locations within the test specimen to monitor excess pore pressure generation, as well as horizontal and vertical particle velocities. The instrumentation locations correspond to a 4-node square element and a position at the center of the element (Figure 4). This sensor configuration facilitates the use of the proposed displacement-based method, as well as the apparent wave method, which requires the wave velocity be evaluated during dynamic testing.

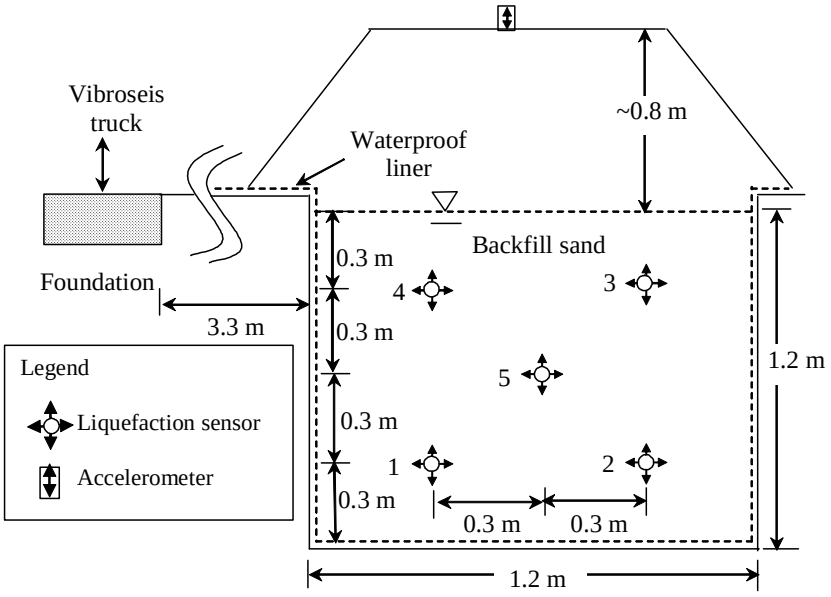

Figure 4. Experimental test set up (not to scale).

Staged testing was performed with the vibroseis, in which small shaking levels first were applied followed by increasing levels of shaking. The staged loading allowed shear strain levels to be compared over a large range of amplitudes (~ 0.0005 to 0.015%). For each stage of loading, a 20-Hz sinusoidal load was applied for 1 second resulting in 20 cycles of load. The loads were applied at 20 Hz because this is the lowest frequency that produces a clean, sinusoidal signal with the current vibroseis truck. The test specimens were allowed to rest for thirty minutes between load stages to allow any excess pore pressure to dissipate.

Mean Shear Strain Amplitudes

Data from one series of in situ liquefaction experiments were used to compare the shear strain computation methods. The comparisons were made at the center of the instrumentation array. For the DB method, the shear strain was computed at this point using the eight displacement-time histories from the 4 corner sensor points (one vertical and one horizontal displacement per sensor) and equation (7). The displacement-time histories were acquired by numerically integrating the recorded particle velocity-time histories and incorporating a baseline correction. The wave propagation-based (WB) methods compute strain at the sensor locations, where particle velocity is measured. To compare with the DB shear strain computed at the center of the array, the WB shear strains were computed at the four corner sensors locations and arithmetically averaged in the time domain to obtain a shear strain time history at the center of the array.

For the PSW method, the $V_{S,hv}$ values used in the shear strain calculation were obtained from crosshole shear wave velocity measurements conducted before dynamic loading. At a depth of 0.3 m, $V_{S,hv}$ was measured as 83 m/s, and at a depth of 0.9 m, it was measured as 109 m/s. For the PRW method, the Rayleigh wave velocity (V_R) was taken as 150 m/s for the applied 20 Hz loading, based on field vibration tests conducted prior to testing. The reason V_R is larger than $V_{S,hv}$ in this experiment is that $V_{S,hv}$ represents waves only traveling in the liquefiable soil, while V_R represents surface waves traveling through both the liquefiable soil and about 5 m of the underlying, stiffer soils. The α_v values were calculated based on the depths of the geophones, a V_R of 150 m/s, and $\nu = 0.25$. The corresponding values of α_v for the sensor depths of 0.3 m and 0.9 m are -1.77 and -1.49, respectively. For the AW method, the apparent phase

velocities (V_{ah}) at the geophone depths (0.3 m, 0.9 m) were computed for each testing stage from the phase difference between the two vertical geophones spaced 0.6 m apart (sensors 4-3 and sensors 1-2 in Figure 4). The measured values of V_{ah} varied somewhat between testing stages, ranging between 120 m/s and 180 m/s. These values are larger than the measured crosshole shear wave velocities.

Figure 5 is a plot of the mean shear strain amplitudes (averaged over the entire shear strain-time history) at the center of the array computed by the WB methods versus those computed by the DB method. For the WB methods, the shear strains in Figure 5 are the result of averaging the strains calculated from the 4 sensor points. The data in Figure 5 represent eight separate testing stages, with over an order of magnitude range in shear strain level. Figure 5 indicates that the AW method matches very well with the DB method, especially for shear strain levels less than 1.0×10^{-2}%. In general, the difference between the AW method and the DB method is less than 10%. The shear strain amplitudes calculated by the PSW and PRW methods have similar values and are 40% to 80% larger than the DB method. Because of the good agreement between the mean shear strains computed by the DB and AW methods, the remainder of this study focused on these two shear strain computation methods.

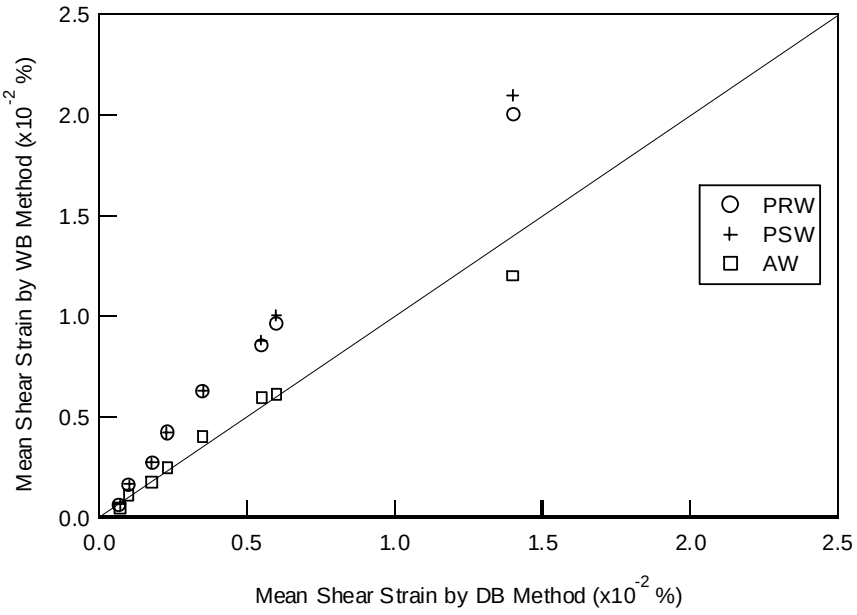

Figure 5. Comparison of mean shear strains computed by wave propagation-based (WB) and displacement-based (DB) methods

Shear Strain-Time Histories

For a more complete comparison of the shear strain computation methods, full shear strain-time histories were evaluated by the DB and AW methods (Figure 6). Two testing stages were chosen for comparison; a small loading level where no excess pore pressure was generated and a large loading level where significant excess pore pressure was generated. In the small loading stage (Figure 6a), the shear strain-time histories computed by the DB and AW methods are very similar throughout dynamic loading and the shear strain amplitudes are relatively constant. However, in the large-strain test (Figure 6b) the shear strain-time histories from the DB and AW methods are noticeably different after about the third loading cycle. The shear strain amplitudes computed by the DB method vary considerably between loading cycles, while the shear strain amplitudes computed by the AW method remain relatively constant. In

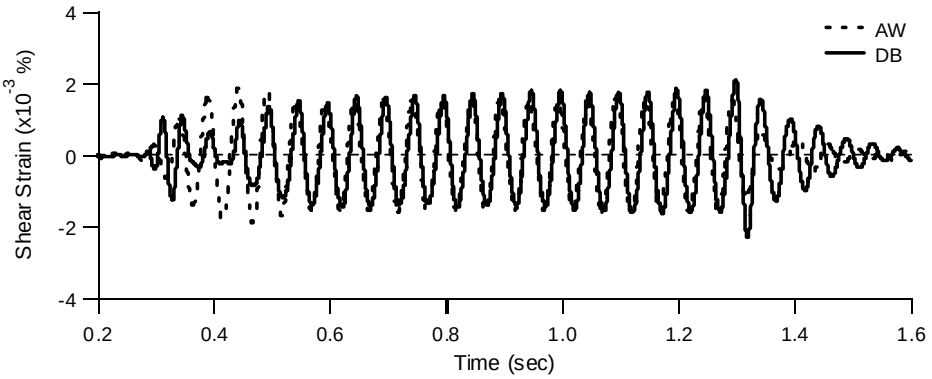

(a)

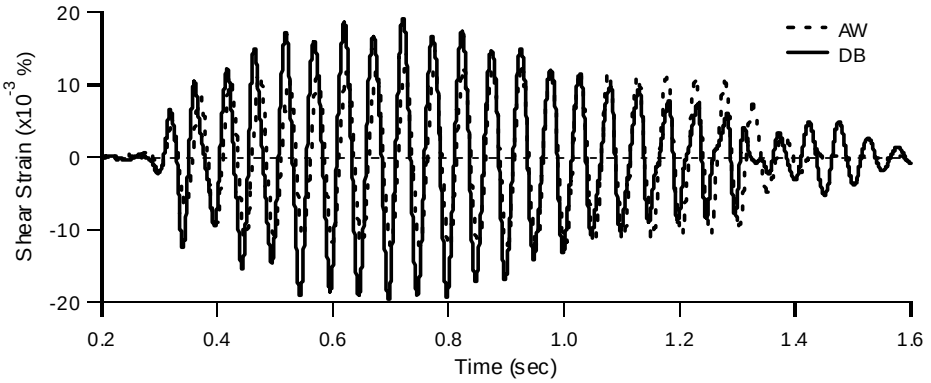

(b)

Figure 6. Shear strain-time histories from the DB and AW methods for a (a) small loading stage and (b) large loading stage.

fact, the peak shear strain from the DB method is about 55% larger than from the AW method. This difference at large loading levels is also seen in Figure 5, where the mean AW shear strain is smaller than the mean DB shear strain for the largest strain level. Consequently, although the mean shear strain amplitudes from the DB and AW methods may be quite similar (Figure 5), the maximum shear strain and the variation in shear strain amplitude between cycles may be different.

Several issues were considered to explain the differences in the shear strain-time histories. The AW method uses only vertical particle velocity data to compute shear strain, while the DB method uses both horizontal and vertical particle velocity data. To demonstrate the effect of the horizontal motion on the shear strains computed by the DB method, the shear strain-time history at the center of the array was computed using both vertical and horizontal displacements, as well as using only vertical displacements. Figure 7 displays the DB shear strain-time history computed from vertical motion only, along with the shear strain-time history resulting from using both horizontal and vertical motions. The two time histories are very similar, particularly during the first three cycles of motion. After about 0.5 s, the contribution from the horizontal component becomes most evident, with the peak shear strain from horizontal and vertical motion about 15% greater than the peak shear strain from only vertical motion. Horizontal motion contributes to the induced shear strain for this experiment because Rayleigh waves are dominating the dynamic loading. The displacement field induced by a Rayleigh wave (Figure 2) includes a variation of the horizontal displacement with depth which contributes to the shearing of the soil. Figure

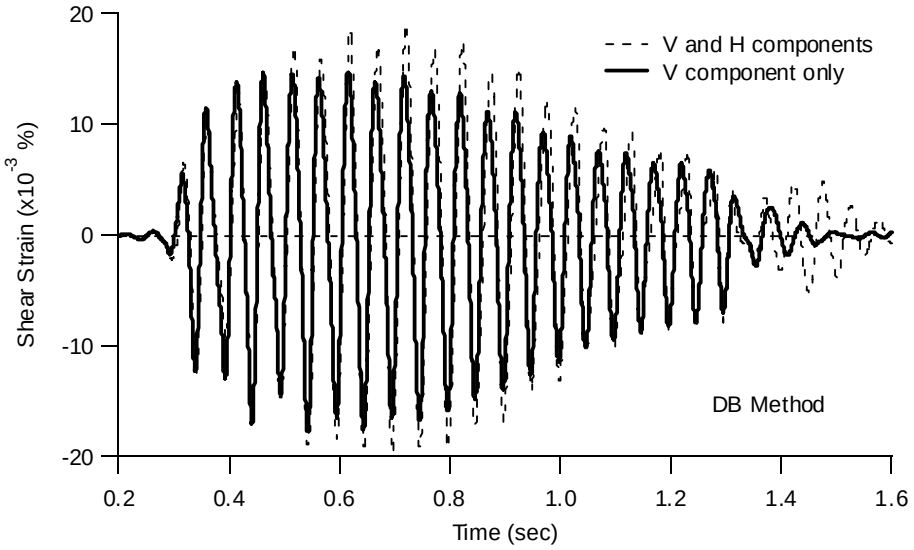

Figure 7. DB method shear strain-time histories computed using vertical motion only and using both vertical and horizontal motions.

7 indicates that using only the vertical component of motion in a DB strain calculation can result in an underprediction of shear strain as large as 15% when Rayleigh waves are the dominant wave type shearing the soil. However, this does not explain the 55% discrepancy observed between the AW and DB methods (Figure 6b).

Another issue to consider when reconciling the shear strains computed by the DB and AW methods is the variation in the apparent wave velocity from loading cycle to loading cycle. For the previous analyses, cross-power spectral analysis was used to calculate an average V_{ah} for the entire stage of loading, and this wave velocity was then used in the AW shear strain calculation. However, it is also possible to compute the apparent wave velocity for each harmonic cycle of motion and use these wave velocities in a cycle-by-cycle AW shear strain calculation. A change in V_{ah} from cycle to cycle indicates a change in phasing between the recordings, which leads to changes in the relative displacement and strain between points.

For the large loading stage analyzed in Figures 6b and 7, the apparent wave velocities between sensors 4 and 3 and sensors 1 and 2 (see Figure 4) for each loading cycle were computed and are shown in Figure 8a. Surprisingly, the apparent wave velocity generally increases with each cycle, particularly after cycle 10. For sensors 4 to 3 (depth 0.3 m), the apparent wave velocity more than doubles during dynamic loading. For comparison, the values of V_{ah} computed when using the entire duration of loading are also shown in Figure 8a. Because these V_{ah} values represent the average phase difference between adjacent sensors over the full duration of loading, they fall in between the minimum and maximum V_{ah} values computed by the cycle-by-cycle method.

The data in Figure 8a also are surprising in that different wave velocities are measured at 0.3 m and 0.9 m depths. If the induced motions were only from a single Rayleigh wave, the wave velocity measured at different depths would be the same. The data in Figure 8a suggest that other wave types are present and are contributing to the motion in the instrumented test pit.

It should be emphasized that the apparent wave velocity is not equal to the shear wave velocity between the sensors, especially for the complicated wave field encountered in the developed testing technique,

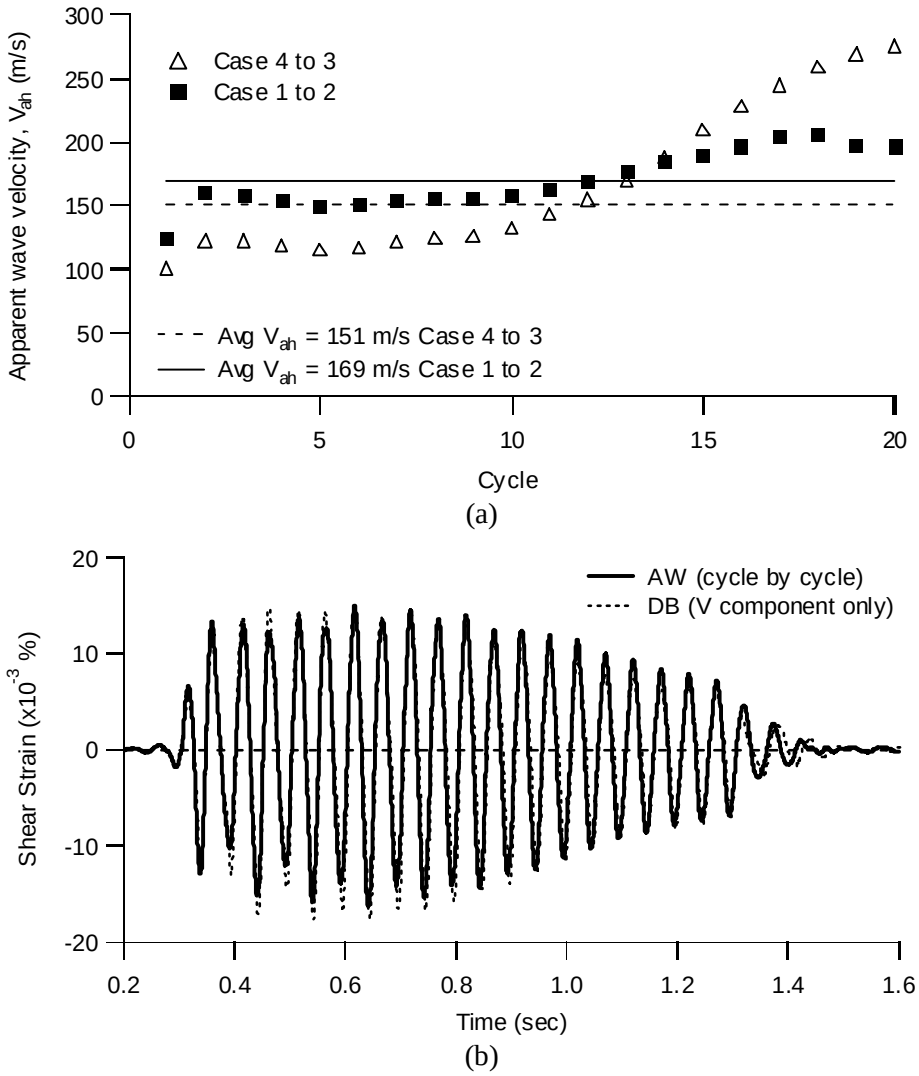

Figure 8. (a) Variation of apparent wave velocity with loading stages, and (b) shear strain-time histories from the DB method and the cycle-by-cycle AW method.

which also includes complications added by the boundary conditions at the edges of the reconstituted test specimen. Therefore, the variation in the apparent wave velocities shown in Figure 8a does not represent the variation in the shear wave velocity or shear stiffness of the test specimen. It is not clear why the apparent wave velocity increases during dynamic loading. One possible explanation is that after a significant amount of pore pressure is induced the wave propagation behavior changes and it causes an increase in apparent wave velocity and a decrease in phase difference between adjacent sensors. This may be the result of the change in the impedance contrast at the edges of the test specimen after significant pore pressure is induced. In contrast to the large loading level where significant pore pressure was induced, the apparent wave velocities did not vary from cycle to cycle in the small stage loading levels where no excess pore pressure was induced. This observation supports the theory that the change in apparent wave velocity is related to pore pressure generation and changes in wave propagation behavior in the test pit.

The apparent wave velocities in Figure 8a were used to compute shear strains on a cycle-by-cycle basis using the AW method. In this calculation, the shear strain at each sensor point was computed using the

vertical particle velocity and the corresponding apparent wave velocity for that cycle. The AW shear strain at the center of the array was computed by averaging the shear strains at the four nodal points. The shear strain-time history at the center of the array using the DB method (vertical motion only) and the cycle-by-cycle AW method are shown in Figure 8b. The results show excellent agreement between the two methods. Additionally, the AW method now shows a reduction in shear strain amplitude during later loading cycles, similar to the DB method. This decrease in shear strain amplitude is due to the increased apparent wave velocity for these cycles and cannot be tracked by the original AW method because it uses only one value of V_{ah}.

One final comparison was made to investigate the accuracy of a two-node DB method. This method requires only particle motion at two adjacent points (e.g., sensors 4 and 3 in Figure 4), and for shear strains the motion is measured in the direction perpendicular to the direction of wave propagation. The two-node DB is most appropriate for one-dimensional wave propagation problems that do not have motion in other directions contributing significantly to the induced strains. For a two-node DB method, the shear strain can be simply evaluated from the displacements at two adjacent points. For example, the shear strain between sensors 4 and 3 in Figure 4 can be expressed as:

$$\gamma_{xz} = \frac{u_{z3} - u_{z4}}{L_{43}} \tag{12}$$

where u_{z3} and u_{z4} are vertical displacements at sensors 3 and 4, respectively, and L_{43} is the distance between sensors 3 and 4. Vertical displacements are used here because this is the direction perpendicular to wave propagation for this experiment.

Figure 9 compares the two-node DB shear strain-time history from sensors 3 and 4 with the cycle-by-cycle AW shear strain-time history for sensor 4. The shear-strain time histories show excellent agreement, indicating that for one-dimensional wave propagation problems the cycle-by-cycle AW method and the two-node DB method produce similar results. However, it is important to monitor the change in wave propagation velocity in the AW method to ensure that the change in phasing can be taken into account to produce accurate shear strain-time histories. This issue is most critical when significant nonlinearity, including liquefaction, is induced in the soil.

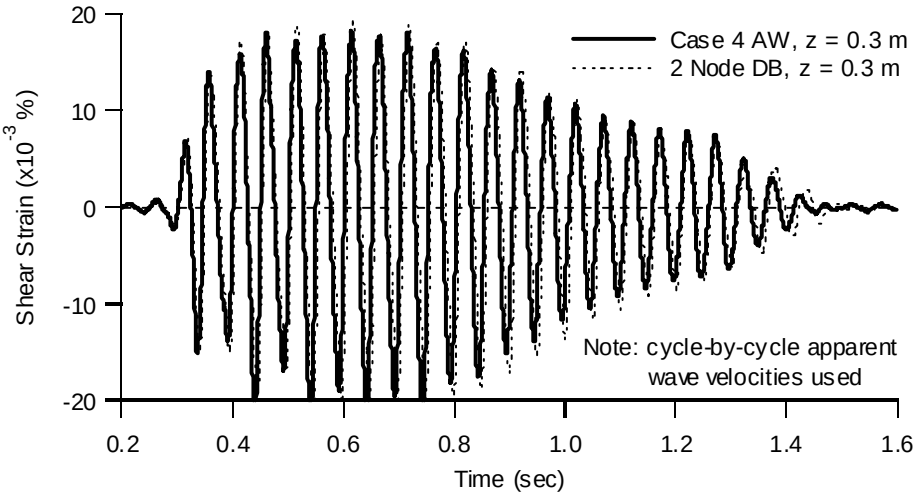

Figure 9. Shear strain-time histories from the two-node DB method and the cycle-by-cycle AW method.

CONCLUSIONS

The evaluation of in situ shear strains induced during dynamic field testing has gained interest recently due to the installation of downhole array instrumentation [e.g., Zeghal et al. 3] and the development of direct in situ liquefaction testing and nonlinear soil property evaluation techniques [e.g., Rollins et al. 1, Rathje et al. 4, Stokoe et al. 2]. The computation of the shear strains induced in the soil relies on measurements of dynamic response (acceleration and/or particle velocity) at various locations in the soil. There are two basic approaches to evaluating strain from dynamic measurements: the displacement-based (DB) approach and the wave propagation-based (WB) approach. The DB approach numerically integrates the measured velocity- or acceleration-time histories to obtain displacement-time histories that are used in conjunction with the solid mechanics definition of strain to compute strain-time histories. When using this approach, the distance between measurement locations should be small relative to the wavelength of the waves shearing the soil. The WB approach computes strain from the ratio of particle velocity to wave velocity. Different directions of particle velocity and types of wave velocities are used to compute various components of strain. This study focused on comparing shear strains computed by the DB method and three WB based methods (plane shear wave, plane Rayleigh wave, and apparent wave methods). Dynamic response measurements from an in situ liquefaction experiment were used for the comparisons.

When comparing mean shear strains over a large range of shear strain levels (0.0005% to 0.02%), the plane shear wave and plane Rayleigh wave WB methods predict shear strain levels 40% to 80% larger than the DB method. However, the apparent wave WB method predicts mean shear strains that are very similar to the DB method. This comparison indicates the importance of using the appropriate wave velocity in a wave propagation-based shear strain evaluation method.

Although mean shear strains computed by the DB and AW methods were similar, details in the full shear strain-time histories did not always agree as well. These differences arise because the DB accounts for two issues that the AW method does not: displacements parallel to the direction of wave propagation and changes in phasing (i.e., apparent wave velocity) between measurement points as significant nonlinearity is induced. For the testing configuration and wave types considered in this study, incorporating the horizontal displacements in the DB strain calculation resulted in a 15% increase in peak strain amplitude. This issue was only significant in this experiment because Rayleigh waves were employed as the dynamic loading and Rayleigh waves induce a displacement field that involves a variation in horizontal displacement with depth. This issue would not be significant for one-dimensional shear wave propagation. For loading levels where significant nonlinearity and/or liquefaction is induced, the phase difference between measurement points changes, which results in changes in the relative displacement between these points and the computed strain levels. This phenomenon can only be captured by the AW method if the apparent wave velocity is computed on a cycle-by-cycle basis. For this study, the cycle-by-cycle AW method produced shear strain-time histories that were in good agreement with the DB method. However, the cycle-by-cycle V_{ah} calculation was facilitated in this study by the fact that a sinusoidal load was applied. This computation would be more difficult if a non-sinusoidal load was used. Consequently, the DB shear strain computation method is preferred because it can best track changes in shear strain amplitude as wave propagation behavior changes. This issue is most important when significant nonlinearity and/or liquefaction are induced.

ACKNOWLEDGMENTS

Financial support was provided by the National Science Foundation under the CAREER award CMS-9875430 and the U.S. Geological Survey under NEHRP grant 00HGGR0015. This support is gratefully acknowledged. P. Axtell, J.Y. Chen, K. Hazirbaba, T.Y. Hsieh, I. Karatas, Y.C. Lin, A. Sharma, and C.

Viyanant all graciously assisted in the field testing. Any opinions, findings and conclusions or recommendations expressed in this material are those of the authors and do not necessarily reflect the views of the National Science Foundation.

REFERENCES

1. Rollins, K.M., Lane, J.D., Nicholson, P.G., Rollins, R.E. "Liquefaction Hazard Assessment using Controlled-Blasting Techniques." Proceedings, 11th International Conference on Soil Dynamics & Earthquake Engineering and 3rd International Conference on Earthquake Geotechnical Engineering, Berkeley, California, USA, 2004, Vol. 2: 630-637.
2. Stokoe, K.H., Axtell, P.J., and Rathje, E.M. "Development of an In Situ Method to Measure Nonlinear Soil Behavior." Third International Conference on Earthquake Resistant Engineering Structures, Malaga, Spain, 2001.
3. Zeghal, M., Elgamal, A.W., Tang, H.T., and Stepp, J.C. "Lotung Downhole Array II: Evaluation of Soil Nonlinear Properties." ASCE Journal of Geotechnical Engineering, 1995, 121(4): 363-378.
4. Rathje, E.M., Chang, W.-J., and Stokoe II, K.H. "Development of an In Situ Dynamic Liquefaction Test." submitted for publication in ASTM Geotechnical Testing Journal.
5. Veyera, G.E., Charlie, W.A., and Hubert, M.E. "One-Dimensional Shock-Induced Pore Pressure Response in Saturated Carbonate Sand," Geotechnical Testing Journal**,** ASTM**,** 2002, 25(3), Paper ID GTJ20029927_253, www.astm.org.
6. Chapra, S.C. and Canale, R.P. "Numerical Methods for Engineers: with programming and software applications, 3rd Edition." McGraw Hill, Boston, MA, 1998.
7. Gohl, W. B., Howie, J.A., and Rea, C.E. "Use of Controlled Detonation of Explosives for Liquefaction Testing." Proceedings, 4th International Conf. on Recent Advances in Geotechnical Earthquake Engineering and Soil Dynamics, San Diego, CA, 2001.
8. Chang, W.-J. "Development of an In Situ Dynamic Liquefaction Test," Ph.D. Dissertation, University of Texas at Austin, 316 pp, 2002.
9. Cook, R.D., Malkus, D.S., and Plesha, M.E. "Concepts and Applications of Finite Element Analysis, 3rd Edition." John Wiley and Sons, New York, NY, 1989.
10. Richart, F. E., Hall, J. R., and Woods, R. D. "Vibration of Soils and Foundations." Prentice-Hall, Inc., New Jersey, 1970.
11. Woods, R. D. "Screening of surface waves in soils," Journal of the Soil Mechanics and Foundations Division, ASCE, 1968, 94(SM4): 951-979.
12. Rayleigh, L. "On waves propagated along the plane surface of an elastic solid." Proceedings of the London Mathematical Society, 1885, 17:4-11.